JOURNAL OF GEOPHYSICAL RESEARCH, VOL. 114, D14110, doi:10.1029/2008JD011173, 2009

Impact of the Indian Ocean subtropical dipole on the precipitation of east China during winter monsoons

Qiuming Yang[1]

Received 19 September 2008; revised 26 February 2009; accepted 28 May 2009; published 31 July 2009.

[1] A link between the Indian Ocean subtropical dipole (IOSD) of sea surface temperature anomalies (SSTA) and rainfall in east China during winter monsoons is unraveled, and the associated physical mechanism has been identified. A sea-air interaction in the southern Indian Ocean (IO) linked to IOSD changes the internal heating distribution of the atmosphere over south Asia and east Asia, and then a low-frequency wave train of the circum-Pacific pattern (CP) around the Pacific Ocean at 500 hPa during the Northern Hemisphere winter is generated, corresponding to a series of anomalous anticyclone and cyclone circulation at 850 hPa. During boreal winter when a positive (negative) IOSD event occurs, a southwestern (northeastern) wind anomaly appears over southeastern China to the south of an anomalous cyclone (anticyclone) circulation, and such a wind anomaly is associated with a strong ascending (descending) motion. As a result, rainfall anomalies in the south of the Yangtze River and northern China tend to be increased (decreased). The impacts of the IOSD on the China climate during winter are very different from those of ENSO, and the difference of the geographical regions for dry/wet conditions in the winter in China influenced by IOSD and ENSO is significant. Hence the CP wave train related to IOSD is one of the key factors resulting in the rainfall anomalies in east China during winter monsoons.

Citation: Yang, Q. (2009), Impact of the Indian Ocean subtropical dipole on the precipitation of east China during winter monsoons, *J. Geophys. Res.*, *114*, D14110, doi:10.1029/2008JD011173.

1. Introduction

[2] East Asia is one of the famous monsoon regions in the world, and the East Asian winter monsoon (EAWM) not only is the most prominent circulation pattern during winter, but also plays an important role in the winter climate of China. With the development of society and economy, more attention has been focused on the winter climate and its effects on agriculture, energy, and water resource. All previous studies have improved our knowledge about EAWM, and have also indicated that ENSO events are an important factor on the intensity of EAWM [*Zhang et al.*, 1996; *Wang et al.*, 2000; *Wang and Zhang*, 2002, and many other studies]. On the other hand, air-sea interaction of the tropical Indian Ocean and its impact on the Northern Hemisphere and Southern Hemisphere circulations have been studied extensively [*Pascal and Dominiak*, 2005; *Liu et al.*, 2006; *Annamalai et al.*, 2007; *Ashok et al.*, 2007; *Huang and Shukla*, 2007, and many other studies], particularly Indian Ocean dipole (IOD) [*Saji et al.*, 1999]. To some extent, EAWM is also related to IOD. However, there were few studies focusing on the effect of the southern Indian Ocean near the monsoon region on EAWM. Through an empirical orthogonal function (EOF) analysis, *Behera and Yamagata* [2001] found that the sea surface temperature (SST) anomalies in the subtropical southern Indian Ocean is characterized as a basinwide dipole pattern with opposite poles off Australia and south of Madagascar, which is usually referred to as the Indian Ocean subtropical dipole (IOSD) mode. They demonstrated that the IOSD mode is phase locked to the Northern Hemisphere winter and generated by surface latent heat flux changes associated with the wind speed fluctuations. *Suzuki et al.* [2004] examined the simulated IOSD in a coupled ocean-atmospheric general circulation model (CGCM). But, it is not clear that the tropical and extratropical circulation anomalies in the Northern Hemisphere, especially in east Asia, are influenced by the IOSD. Another important unresolved issue is the important role of the IOSD in the winter climate of China and its difference from the ENSO.

[3] Significant heating anomalies during the peak phase of the IOSD would not only caused the anomalies of the tropical-extratropical circulation in southern Indian Ocean, but also caused the convection heating and the anomalies of the a larger-scale flow pattern at low latitudes in South Asia and East Asia. Moreover, the impacts of the IOSD on the climate over mid-high latitudes in East Asia may be attributed to the low-frequency wave train generated by the tropical-extratropical interaction in East Asia. Thus it is importance to understand and interpret these responses in terms of theoretical framework and practical applications.

[4] In this study, we investigate the possible of the influence of the variability of the IOSD on the climate of

[1]Laboratory of Weather and Climate, Jiangsu Meteorological Institute, Nanjing, China.

0148-0227/09/2008JD011173$09.00

east China during winter monsoons, as well as the possible mechanism.

2. Data and Methods

[5] The Hadley Centre Global Sea Ice and Sea Surface Temperature (HadISST) Analyses data sets [*Rayner et al.*, 2006], from January 1951 to February 2007 were used in this study. For precipitation analysis, we mainly use the reconstructed rainfall data over land based on gauge observations (PREC/L) from 1948 to 2007 on a 2.5° grid [*Chen et al.*, 2002] and the data sets of Version 2 Global Precipitation Climatology Project Monthly Precipitation Analyses from 1979 to 2007 [*Adler et al.*, 2003]; Atmospheric circulation fields were obtained from the National Center for Environmental Prediction/National Center for Atmospheric Research (NCEP/NCAR) reanalysis data set for the period of 1951–2007 [*Kalnay et al.*, 1996]. The monthly indices and anomaly fields have been seasonally averaged over a period from December to February to obtain what we hereafter refer to as the Northern Hemisphere winter values.

[6] We first defined as the SST anomaly that the dipole mode may be identified by a simple index time series which describes the difference normalized SST anomaly between the northern-eastern (22.5°S–27.5°S, 97.5°E–102.5°E) and southern-western (32.5°S–37.5°S, 62.5°E–72.5°E) over subtropical southern Indian Ocean, referred to as the dipole mode index (IOSDI). Then, we studied the teleconnections between the IOSDI and the rainfall in China and the global 500-hPa geopotential height for the Northern Hemisphere winter. Moreover, the coupled correlation patterns between the global winter circulation and IOSD were identified by a conditional singular value decomposition (CSVD) analysis, i.e., conditional maximum covariance analysis (CMCA) [*An*, 2003], in which the background state signals of the circulation have been excluded. On the basis of the data of the winter 500-hPa geopotential height, vertical velocity (ω), 200-hPa wind vector, 850-hPa wind vector and horizontal moisture flux vector ($Q = (qu, qv)$, where q is the specific humidity), the spatial distributions of the China rainfall and circulation and water vapor anomalies corresponding to the peak years with IOSDI values being greater (less) than one positive (negative) standard deviation were studied by the composite analyses, and the possible mechanisms were also discussed.

3. Indian Ocean Subtropical Dipole (IOSD) and Rainfall of East China During Winter Monsoons

3.1. Relationship Between IOSD and Rainfall in East China During the Northern Hemisphere Winter

[7] The second mode of SSTA in southern IO is characterized by the signature of the IOSD (not shown). There is a strong correlation (0.918) between IOSDI (Figure 1a) and - PC2 (the time series of this mode) with the significant at 99.9% confidence level. On the basis of correlation analysis, it is seen that there is an opposite poles off Australia and south of Madagascar with a significant anomalous subtropical zonal SST gradients (Figure 1b). The maximum correlations are significant at 99% confidence level. This indicates the IOSDI is in good agreement with the variation of IOSD mode. In addition, the relatively weak anomaly appears in the eastern equatorial Pacific, which is significant at 95% confidence level, but there is no anomaly signal over the tropical Indian Ocean. This connection implies that, to some extent, IOSD is also linked to ENSO.

[8] Figure 1c shows the correlation map between the winter IOSDI and precipitation in China for the period of 1951–2006 (used the reconstructed rainfall for PREC/L). There are areas with significantly positive correlation in the south of the Yangtze River valley and the northern China, which are statistically significant at a 95% confidence level from a two-tailed Student's *t*-test, and significant at a 99% confidence level in some parts of southern China (near Guangdong). Moreover, Figure 1d gives the correlation map of the winter IOSD with rainfall in the whole of the Indo-Pacific domain (used the data sets of Version 2 Global Precipitation Climatology Project Monthly Precipitation Analyses [*Adler et al.*, 2003] for the period 1979–2006). During boreal winter, as seen in Figure 1d, IOSD has significant correlations with the local rainfall as well as that over other areas; in particular, it is evidently positively correlated with rainfall over the region from the south of the Yangtze River valley into northwestern Pacific (the maximum correlation over in some parts of the southern China with the significant at 99% confidence level), which is in agreement with Figure 1c. It is important to notice that the relatively weaker positive correlation is also seen over the eastern tropical Pacific (with the significant at 95% confidence level), but the stronger negative correlations are over the western tropical Pacific (with the significant at 99% confidence level). Therefore the above (below)-normal rainfall over the south of the Yangtze River valley is associated with a positive (negative) IOSDI during the Northern Hemisphere winter. This seems to suggest that the IOSD may be an important role in the rainfall anomalies of east China during winter monsoon.

3.2. Wave Train Bridge Between the Southern Subtropical Indian Ocean and East China

[9] In the previous section, it was confirmed that there is a significant positive correlation between the IOSD index and the rainfall in east China during winter monsoons. In this section, we show that a wave train bridge may provide the causal relationship that results in the correlations. Figure 2 shows the correlations of the IOSDI with global geopotential anomalies at 500 hPa during the Northern

Figure 1. (a) Normalized time series of the winter IOSD index and (b) correlations with SST anomaly in the Indo-Pacific for the period 1951–2006. Values are multiplied by100, and the contour interval is 10. The regions above the 95% significant level are shaded. (c) Correlation field between the Indian Ocean subtropical dipole (IOSD) and the precipitation in China for the period 1951–2006 during the Northern Hemisphere winter. Values are multiplied by 100, and the contour interval is 10. Light (dark) shaded areas represent correlations lower (greater) than −0.27 (+0.27) with the 95% significance level for nonzero correlation (using a two-tailed *t*-test). (d) Same as Figure 1c but for the precipitation over the Indo-Pacific during the period 1979–2006.

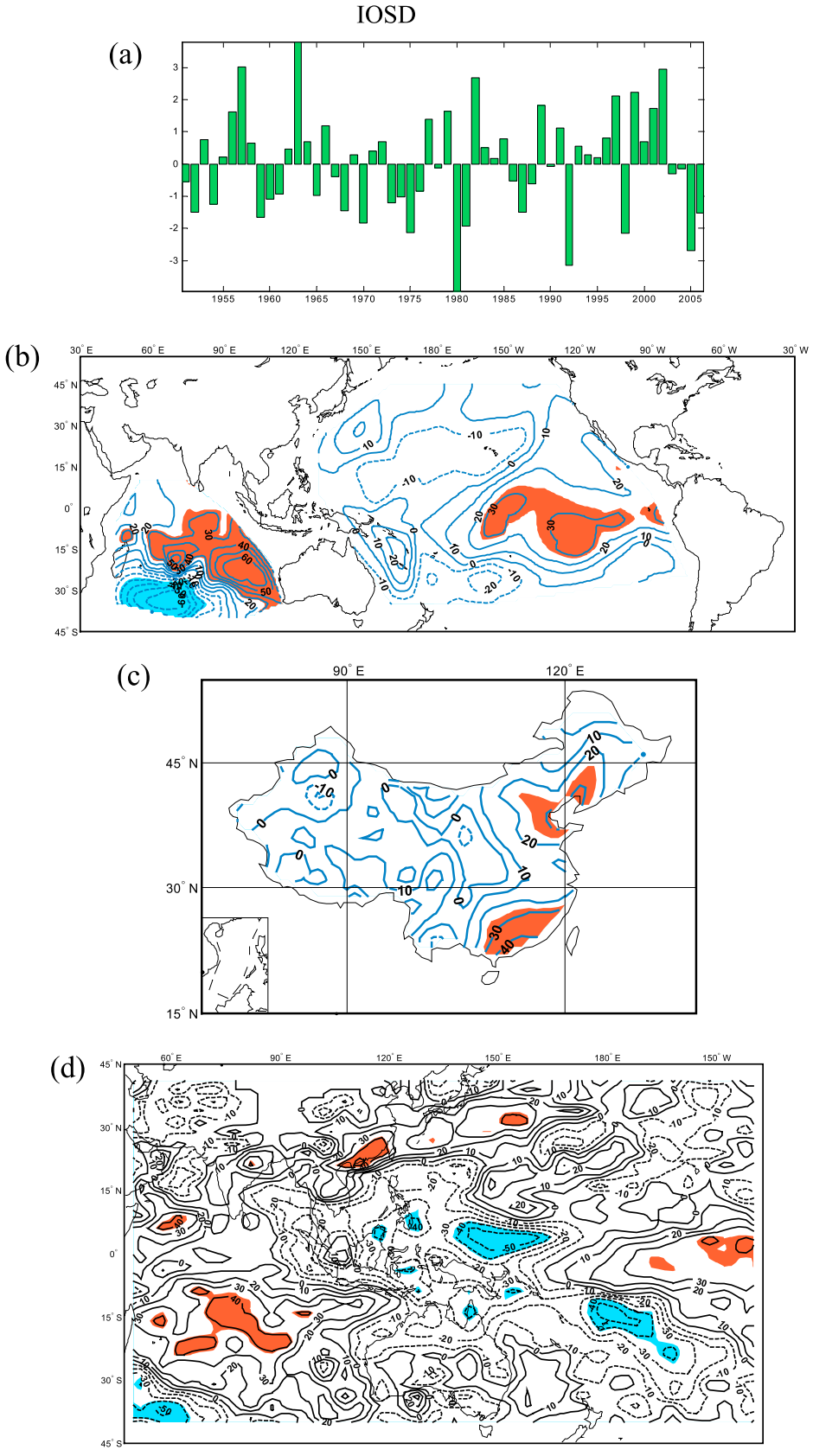

Figure 1

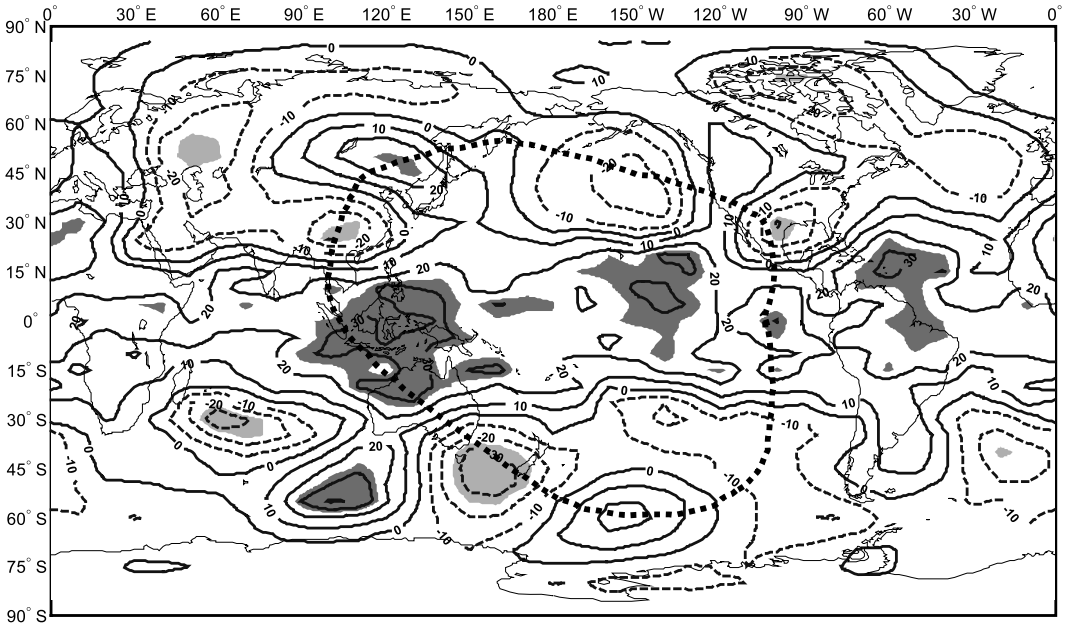

Figure 2. Correlation field between the Indian Ocean subtropical dipole (IOSD) and the global 500-hPa geopotential height anomalies for the period 1951–2006 during the Northern Hemisphere winter. Values are multiplied by 100, and the contour interval is 10. Light (dark) shaded areas represent correlations lower (greater) than −0.27 (+0.27) with the 95% significance level for nonzero correlation (using a two-tailed *t*-test).

Hemisphere winter. The high-correlation regions concentrate on the mid-high latitudes over the southern Indian Ocean, western Pacific and the south of Eurasia continent, eastern tropical Pacific and western tropical Atlantic. It is interesting to note that the correlation of the dipole structure for height anomalies in southern Indian Ocean corresponds well to the dipole-like SSTA distribution (IOSD) with the significant at 95% confidence level (estimated by a two-tailed *t*-test). These results are consistent dynamically, which are related to sea-air interaction in this region. Significant negative correlations can also be seen over middle latitude in the south Atlantic. Another major feature is that there is a significant low-frequency wave train of circum-Pacific pattern (CP) around Pacific, which is similar to CPTP of the 100-hPa annual meridional wind [*Wang*, 2005] but the position of the CP pattern shifts further westward, which is not composed of the North Pacific-North American teleconnection (PNA) pattern [*Wallace and Gutzler*, 1981; *Ghil and Mo*, 1991a, 1991b] and the South Pacific-South American teleconnection (PSA) pattern [*Mo and White*, 1985; *Ghil and Mo*, 1991a, 1991b; *Mo and Higgins*, 1998]. Significant positive correlations are seen over high latitude in southern Pacific, the north of the Australia, western tropical Pacific, the northern China, tropical Atlantic and northern Brazil, while significant negative correlations are seen over the middle latitude in southern Pacific, the central and east China, northeastern Pacific and the south of North America. Composite analysis for the positive (negative) IOSD years, with IOSDI values being greater (less) than one positive (negative) standard deviation of the index, also prove the existence of the CP pattern. The spatial distribution of the global 500-hPa height anomalies for the composite IOSD anomalous event formed by the difference between the observed ten positive (1956, 1957, 1963, 1979, 1982, 1989, 1997, 1999, 2001 and 2002) and eight negative (1959, 1970, 1975, 1980, 1981, 1992, 1998 and 2005) events during the Northern Hemisphere winter (not shown). It turns out that a chain of alternating anomalies exists roughly around the Pacific, showing that a noticeable CP pattern is well organized.

[10] To elaborate the linear relationship between the global winter circulation and IOSD, a singular value decomposition (SVD) analysis [*Wallace et al.*, 1992] is also applied to the winter global 500-hPa geopotential height anomalies and SSTA over southern subtropical Indian Ocean for the period 1951–2006. In this analysis, the height and SST data from which the first EOF of the 500-hPa height anomalies was removed, and the background state signals related to height anomalies have been excluded. The method above was also referred to the conditional maximum covariance analysis (CMCA) [*An*, 2003] or conditional singular value decomposition analysis (CSVD). The first

Figure 3. (a) Spatial patterns of the second SVD coupled mode of the winter global 500-hPa height anomalies and (b) the SSTA in the subtropical southern Indian Ocean for the period of 1951–2006. Spatial patterns are homogeneous correlation maps and values are multiplied by 100. The contour interval is 10, and negative contours are shown as dashed lines. Light (dark) gray shaded areas represent the negative (positive) correlation with the 95% significance levels, respectively. (c) The expansion coefficient of height (thin line) and SSTA (dashed line). (d) As in Figure 3b but for the correlation between the expansion coefficient of SSTA over the southern IO and over the Indo-Pacific.

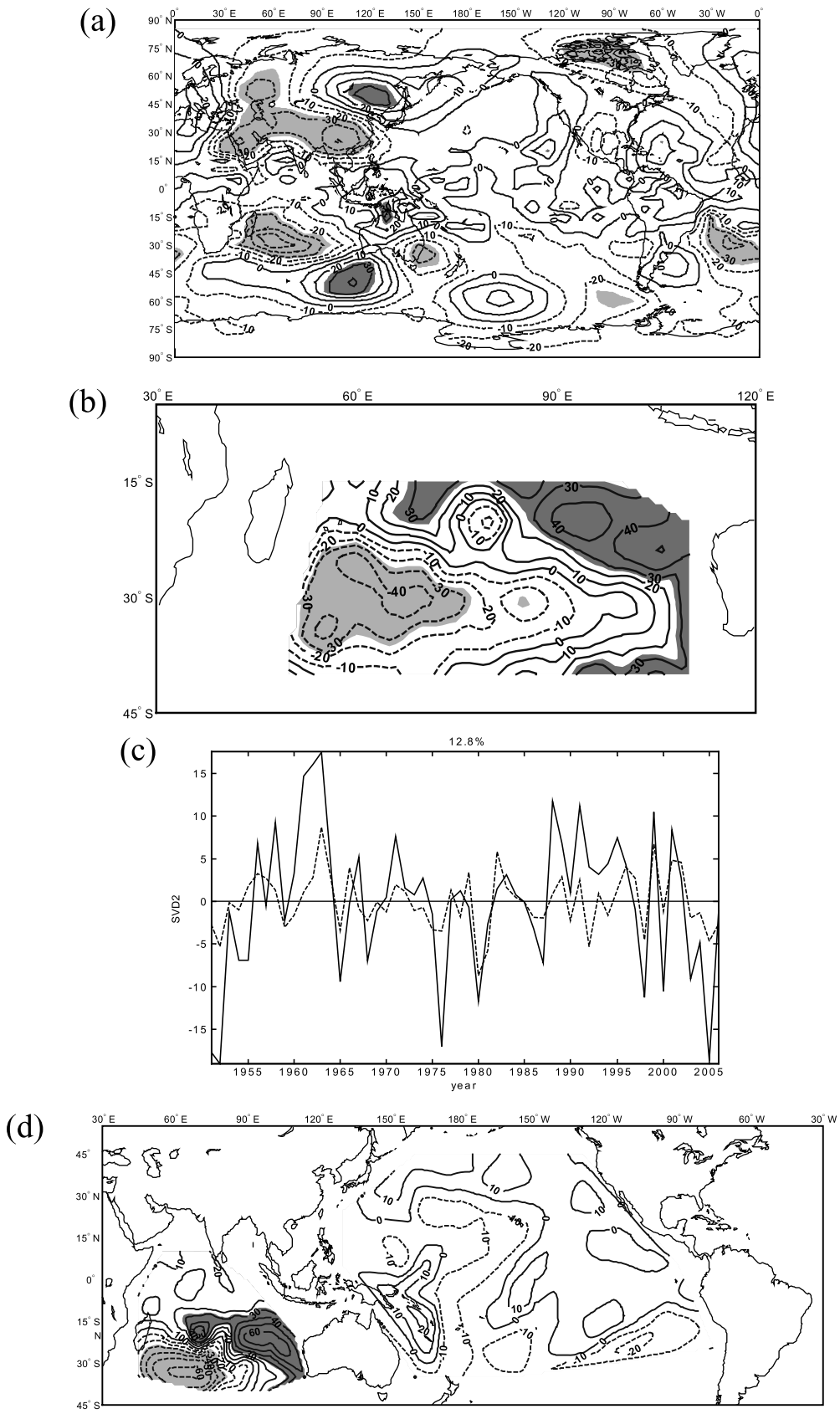

Figure 3

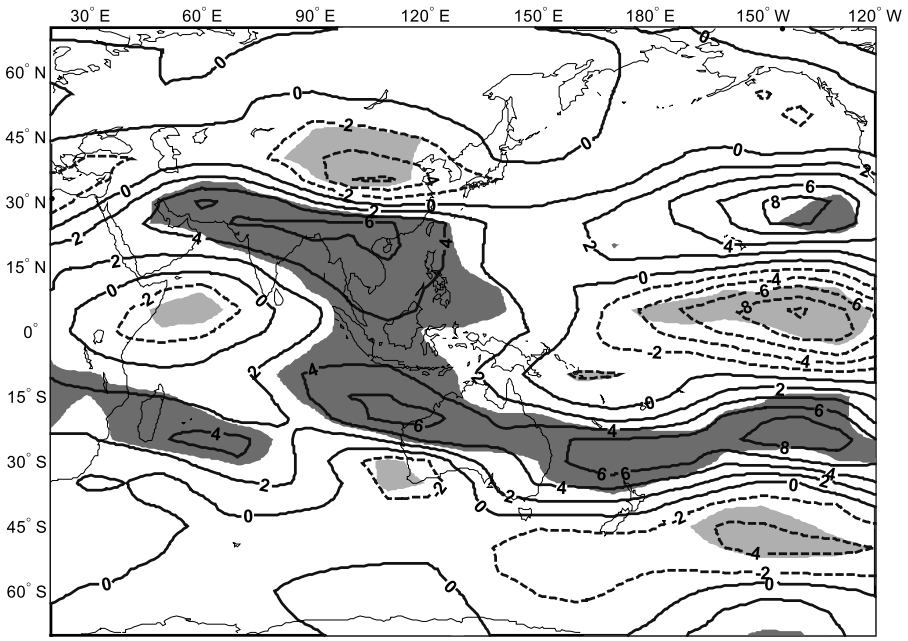

Figure 4. Composite difference of the winter 200-hPa zonal wind (in m s^{-1}) between the stronger positive and negative IOSD years, which are defined in the text. Areas exceeding the 95% *t*-test significance level are shaded.

SVD mode is related to SH annular mode or AAO (Antarctic Oscillation) [*Gong and Wang*, 1999; *Thompson and Wallace*, 2000] and basin-scale zonal SST anomalies over southern subtropical Indian Ocean (not shown), which accounts for 55.5% of the total squared covariance. The second SVD mode accounts for 12.8% of the total squared covariance, and the global 500-hPa height pattern of this SVD mode is characterized by the signature of the CP pattern (Figure 3a) and SST anomaly pattern shows an appearance with the IOSD (Figure 3b). Further, Figure 3d gives the correlation between SVD time series of SSTA over the southern IO and SSTA over the Indo-Pacific. It is seen that there are no significant signals in the Pacific, and maximum correlation region is located over the southern IO (with the significant at 99% confidence level). The temporal correlation coefficient between the corresponding expansion coefficients (Figure 3c) is 0.671(significant above 99.9% confidence level). This result is in conformity with the conclusion from Figure 2 and confirms further the strongly positive correlation relationship between the winter CP and IOSD. Thereby, the evolution of the circular wave train above reflects the remote linear response of global atmosphere circulation to IOSD, which is closely linked to changes of the internal heating distribution of the atmosphere over south Asia and east Asia caused by the sea-air interaction in the southern IO. When the smaller tropical SSTA anomalies linked to IOSD appears, it may be to induce the nonlinear changes in convergence/divergence patterns in global tropics, especially in the western tropical Pacific, that in turn act as Rossby wave source. Through the middle and low-latitude interaction, the stronger response in the extratropics in both hemispheres occurs, influencing on circulation and the climate the surrounding Pacific region. In this sense, the effect of IOSD has a global structure.

[11] Naturally, the changes of the winter rainfall are well related to simultaneous atmospheric circulation anomalies. The winter east Asian jet (EAJ), especially its location, has been known to play a very strong dynamical role on the precipitation variability [*Yang et al.*, 2002]. Figure 4 exhibits the composite difference of the winter 200-hPa zonal wind anomalies between the positive and negative IOSD years, which are defined earlier. The larger anomalies regions of the meridional wind at 200 hPa are over the tropical southern IO, south Asia and the middle latitude of Asia. These anomalies are associated directly with IOSD. There is positive difference over the south of 30°N, which is concurrent with negative difference over the north of 30°N in east Asia. These changes indicate that the EAJ location shifts southwestward (climatological location of EAJ core is located at around 30°N) and EAWM is weakened, which favors more winter precipitation in south of the Yangtze River, when winter IOSD is positive (Figures 1c and 1d). On the contrary, the EAJ location shifts northeastward and EAWM is intensified under the negative IOSD years, which is disadvantageous for the winter rainfall in south of China. Therefore the anomaly of the IOSD plays a conspicuous role in the EAJ location, which may lead to anomalous rainfall in east Asia in winter. Furthermore, a significantly meridional wave train appears near the central Pacific, which the dynamic mechanism of the process is not clear and needs to be further studied.

[12] The composite difference of the winter 500-hPa vertical velocity (ω) between positive and negative IOSD year is depicted in Figure 5a (larger than zero denotes airflows descending, and less than zero denotes airflows ascending). When winter IOSD is positive, negative anomalies are predominated over the south of the Yangtze River valley where airflows ascend, and positive anomalies are prominent over the tropical western Pacific along 5°N

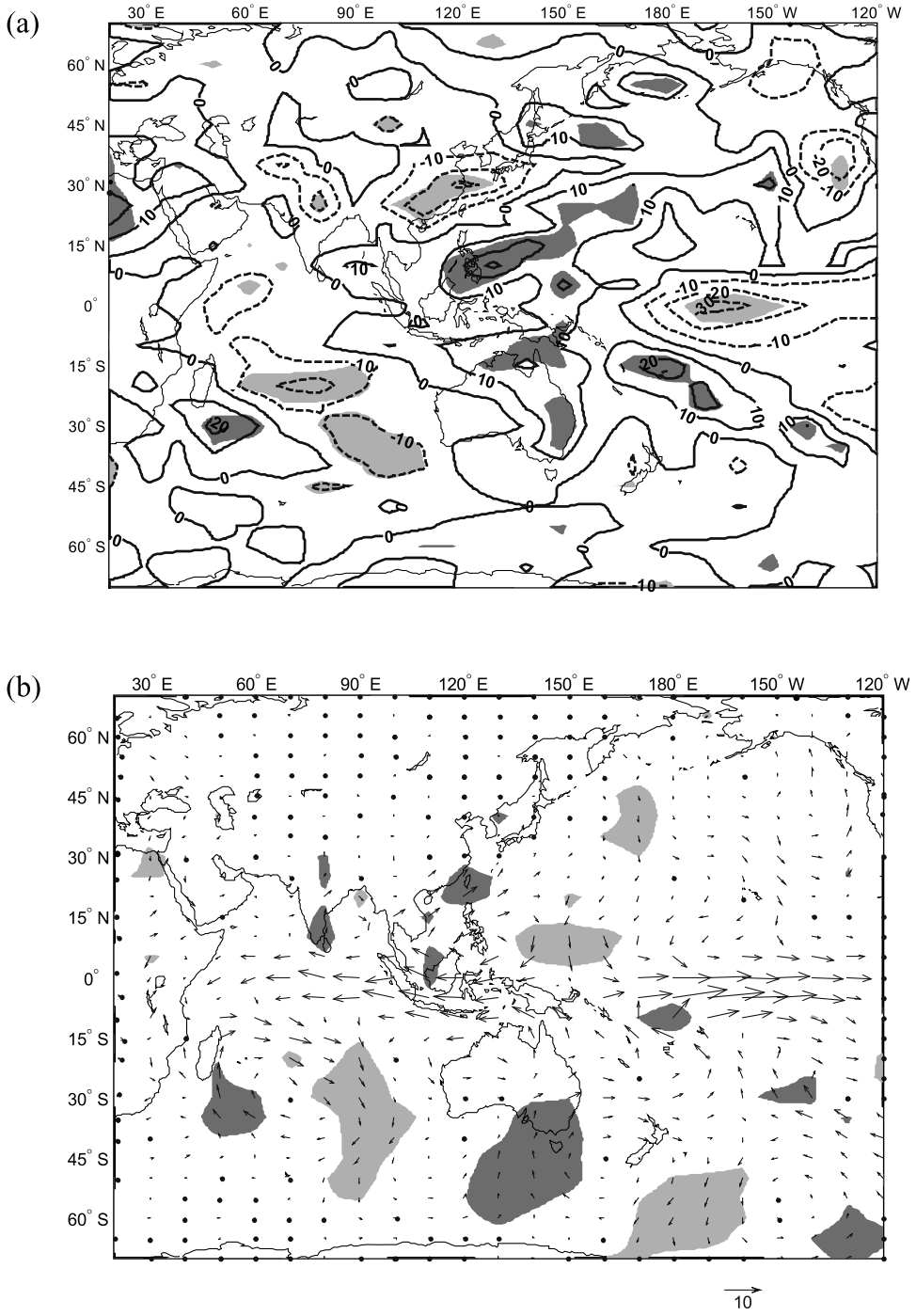

Figure 5. (a) Same as Figure 4 except for the 500-hPa vertical velocity anomalies. The contour interval is 0.001 hPa s^{-1}. Areas exceeding the 95% *t*-test significance level are shaded. (b) Same as Figure 4 except for the 850-hPa horizontal moisture flux vector (in units of g kg^{-1} m s^{-1}), which is significant at the 95% *t*-test confidence level in meridional component (shaded).

where airflows descend. This situation is favorable to the increase of the precipitation in the southern China. When winter IOSD is negative, the situations are reversed with negative anomalies dominating the tropical western Pacific and positive anomalies occupying the south of the Yangtze River valley, thus resulting in the decrease of the precipitation in east China. Moreover, the water vapor conditions change with the anomalous winter atmospheric circulations.

Figure 5b depicts composite difference of the 850-hPa horizontal moisture flux vectors $Q = (qu, qv)$. It can be seen that there exist positive meridional moisture flux anomalies from the southeastern China into northern Philippines (Figure 5b). So the meridional moisture flux is increased and plenty of moisture emerges over east China during positive winter IOSD phase, offering abundant vapor conditions for the precipitation augmentation in this region.

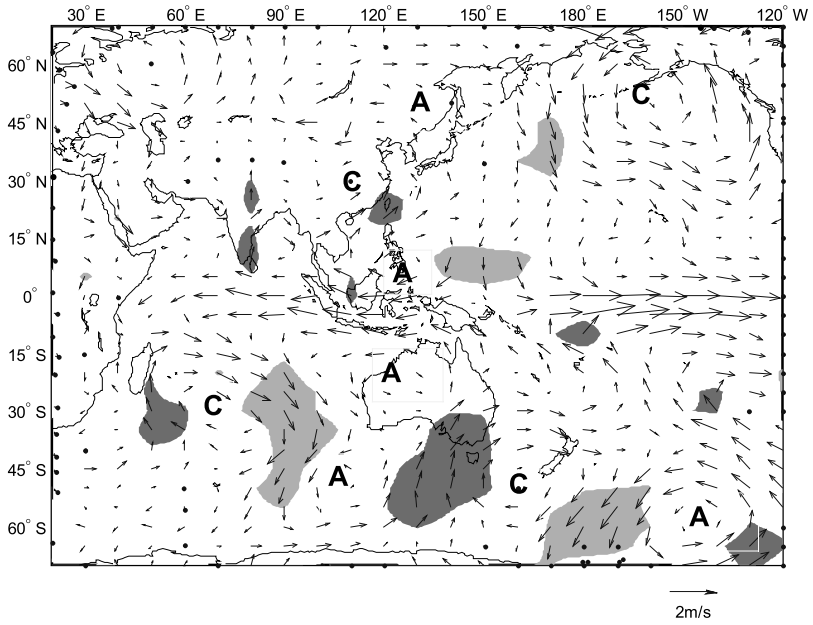

Figure 6. Composite difference of the winter 850-hPa wind vector anomalies between the stronger positive minus negative IOSD years, which are defined in the text. Vectors (m s^{-1}) that are significant at the 95% *t*-test confidence level in *v*-component are shaded. Cyclonic and anticyclonic anomalies are marked with "**C**" and "**A**" respectively.

Whereas the negative winter IOSD phase brings the opposite conditions to that mentioned above.

[13] Consistent with the CP wave train at 500 hPa, there are a series of the anomalous anticyclone and cyclone circulation anomalies around Pacific region for the composite difference of the 850-hPa wind vector between positive and negative IOSD year (Figure 6). It should be noted that these anomalous circulation associated with IOSD are two anticyclones in the western Pacific and Indian Ocean, i.e., one over the south Indian Ocean (SIO), and the other over the western Pacific (WP). These off-equatorial anticyclones are remarkably asymmetrical about the equator, which local atmosphere-ocean interaction is primarily responsible for the amplification and maintenance of the anticyclones in SIO and WNP. This process is implemented through the positive feedback between moist atmospheric Rossby wave and mixed layer ocean [*Wang et al.*, 2003]. Meantime, a remarkable southerly wind anomaly at 850 hPa appears in the Indo-China Peninsula and south coast of China, and such a low-level wind anomaly brings more moisture to east China (Figure 5b), which is associated with a strong ascending motion (Figure 5a). Correspondingly, EAJ shifts to the southwest at 200 hPa (Figure 4) and EAWM is weakened. As a result, some regions of east China receive above normal rainfalls with anomalous centers over the south of Yangtze River valley and the northern China in winter (Figure 1c), which is significant at the 95% level. Thereby, IOSD-related CP pattern is one of the major factors for the influencing interannual variations of the rainfall in east China in the Northern Hemisphere winter.

[14] Additionally, the correlations of the rainfall in China winter and the global 500-hPa geopotential height anomalies to ENSO demonstrate that it is very distinct from the IOSD. Figure 7a gives the correlation field between the first principal component of the SST anomaly over Pacific Ocean (ENSO) and the precipitation in China for the period 1951–2006 during the Northern Hemisphere winter. It is clearly seen from Figure 7a that there are areas with significantly positive correlation in the south of the Yangtze River valley and the southwestern China (near Yunnan), and negative correlation in central China (near Shaanxi) also is more significant, which is different to the correlations of Figure 1c. Unlike the predominant CP pattern associated with the IOSD, the teleconnection of the boreal winter 500-hPa height anomalies to ENSO displays a significant positive correlation region covering most of the global tropics (at a 99.9% significance level) and pronounced PNA pattern in extratropics in the Northern Hemisphere (Figure 7b). Although there is the relatively weaker correlation of IOSD to ENSO (correlation coefficient is 0.275 and only at a 95% significance level), the influences on rainfall over China in winter are different. More importantly, these two phenomena also have very different temporal features. IOSD has an interannual signal with 6.6 year periodicity (at a 99% significance level, based on the noninteger spectrum analysis [*Schickedanz and Bowen*, 1977]), which is different from ENSO with about 3–5 year periodicity. It reflects a unique mode on the sea-air interaction in Indian Ocean. Clearly, teleconnection paths between the two phenomena and rainfall anomalies in China winter are very different.

4. Conclusion and Discussion

[15] In this study, we have examined the association of the interannual variability of IOSD with the Asian atmospheric circulations, particularly with precipitation in east

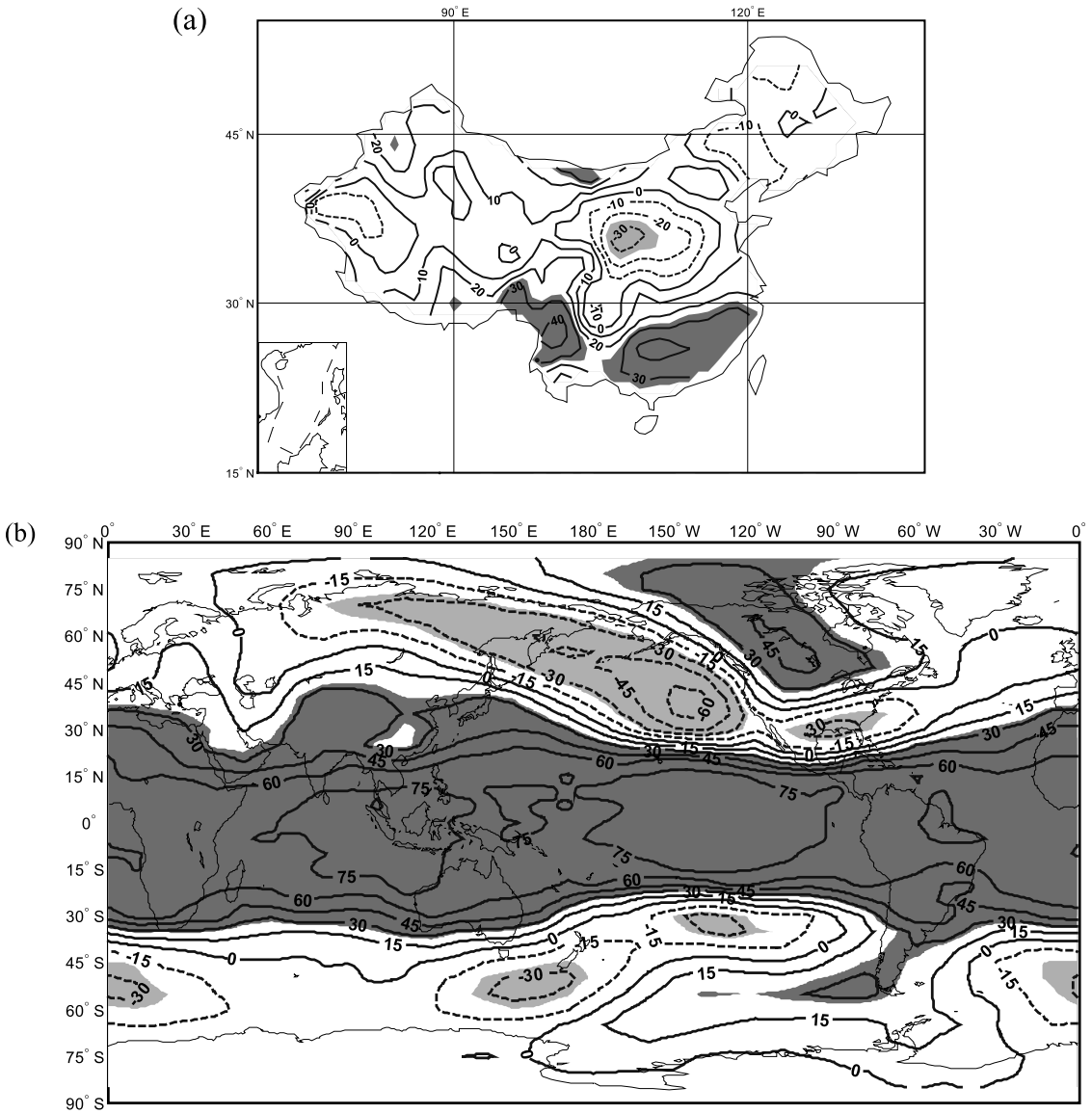

Figure 7. (a) Correlation field between the first principal component of the SST anomaly over the Pacific Ocean (ENSO) and the precipitation in China for the period 1951–2006 during the Northern Hemisphere winter. Values are multiplied by 100, and the contour interval is 10. Light (dark) shaded areas represent correlations lower (greater) than −0.27 (+0.27) with the 95% significance level for nonzero correlation (using a two-tailed *t*-test). (b) Same as Figure 7a except for the global 500-hPa geopotential height anomalies, and the contour interval is 15.

China during winter monsoons. We have further addressed the possible mechanism of their linkage as well.

[16] The result has shown clear evidence that there is a prominently positive correlation between the IOSD and rainfall in east China during the Northern Hemisphere winter, namely, positive (negative) IOSD is accompanied by much more (less) winter rainfall in the south of the Yangtze River valley and northern China. This may be caused by an atmospheric wave train forced by IOSD. The sea-air interaction in southern IO linked to IOSD changes the internal heating distribution of the atmosphere over south Asia and east Asia, and then a low-frequency wave train of circum-Pacific pattern (CP) around Pacific Ocean at 500 hPa during the Northern Hemisphere winter is generated, corresponding to a series of the anomalous anticyclone and cyclone circulation at 850 hPa over east Asia and western Pacific. For the positive IOSD event, there is a southwestern wind anomaly over southeastern China to south of anomalous cyclone circulation. This wind anomaly is associated with the strong ascending motion and southwestward located EAJ and positive meridional moisture flux anomalies at lower level and weaker EAWM, leading to the rainfall anomalies in the south of the Yangtze River valley increased, and *vice versa*.

[17] However, the impacts of the IOSD on the China rainfall in winter are different from those of ENSO, and there are in central (southwestern) part of China for dry (wet) conditions associated with ENSO. It is evident that the teleconnection paths are also very different. But, this possible mechanism needs to be further studied in future

research. In addition, other processes may also be related in the linkage between IOSD and winter rainfall in east China. To demonstrate the roles of the air-sea interaction in generation and maintenance of the CP teleconnection pattern requires a time-dependent calculation with a coupled atmosphere-ocean model. Much research is needed in this regard to further our understanding of the dynamics of the IOSD and the teleconnection to rainfalls of east China during winter monsoons.

[18] **Acknowledgments.** The NCEP/NCAR reanalysis data were obtained from the Climate Diagnostics Center (http://www.cdc.noaa.gov), the Hadley Centre Global Sea Ice and Sea Surface Temperature (HadISST) Analyses data sets were obtained from the East Anglia University in Britain (http://www.cru.uea.ac.uk), and the reconstructed rainfall data over land based on gauge observations (PREC/L) were also obtained from the Climate Diagnostics Center (http://www.cpc.ncep.noaa.gov/products/global_precip/html/wpage.50yrrec.html). The author appreciates the valuable comments and helpful suggestions from two anonymous reviewers.

References

Adler, R. F., et al. (2003), The version 2 Global Precipitation Climatology Project (GPCP) monthly precipitation analysis (1979–present), *J. Hydrometeorol.*, *4*, 1147–1167.

An, S.-I. (2003), Conditional maximum covariance analysis and its application to the tropical Indian Ocean SST and surface wind stress anomalies, *J. Clim.*, *13*, 2044–2055.

Annamalai, H., H. Okajima, and M. Watanabe (2007), Possible impact of the Indian Ocean SST on the Northern Hemisphere circulation during El Niño, *J. Clim.*, *20*, 3164–3189.

Ashok, K., H. Nakamura, and T. Yamagata (2007), Impacts of ENSO and Indian Ocean dipole events on the Southern Hemisphere storm-track activity during austral winter, *J. Clim.*, *20*, 3147–3163.

Behera, S. K., and T. Yamagata (2001), Subtropical SST dipole events in the southern Indian Ocean, *Geophys. Res. Lett.*, *28*, 327–331.

Chen, M., P. Xie, J. E. Janowiak, and P. A. Arkin (2002), Global land precipitation: A 50-yr monthly analysis based on gauge observations, *J. Hydrometeorol.*, *3*, 249–266.

Ghil, M., and K. C. Mo (1991a), Intraseasonal oscillations in the global atmosphere. Part I: Northern Hemisphere and tropics, *J. Atmos. Sci.*, *48*, 752–778.

Ghil, M., and K. C. Mo (1991b), Intraseasonal oscillations in the global atmosphere. Part II: Southern Hemisphere, *J. Atmos. Sci.*, *48*, 780–790.

Gong, D., and S. Wang (1999), Definition of Antarctic oscillation index, *Geophys. Res. Lett.*, *26*, 459–462.

Huang, B., and J. Shukla (2007), Mechanisms for the interannual variability in the tropical Indian Ocean. Part II: Regional processes, *J. Clim.*, *20*, 2937–2960.

Kalnay, E., et al. (1996), The NCEP/NCAR 40-year reanalysis project, *Bull. Am. Meteorol. Soc.*, *77*, 437–471.

Liu, X., Z. Liu, J. E. Kutzbach, S. C. Clemens, and W. L. Prell (2006), Hemispheric insolation forcing of the Indian Ocean and Asian monsoon: Local versus remote impacts, *J. Clim.*, *19*, 6195–6208.

Mo, K. C., and G. H. White (1985), Teleconnections in the Southern Hemisphere, *Mon. Weather Rev.*, *113*, 22–37.

Mo, K. C., and R. W. Higgins (1998), The Pacific-South American modes and tropical convection during the Southern Hemisphere winter, *Mon. Weather Rev.*, *126*, 1581–1596.

Pascal, T., and S. Dominiak (2005), Indian Ocean sea surface temperature and El Niño-Southern Oscillation: A new perspective, *J. Clim.*, *18*, 1351–1368.

Rayner, N. A., et al. (2006), Improved analyses of changes and uncertainties in marine temperature measured in situ since the mid-nineteenth century: The HadSST2 data set, *J. Clim.*, *19*, 446–469.

Saji, N. H., B. N. Goswami, P. N. Vinayachandran, and T. Yamagata (1999), A dipole mode in the tropical Indian Ocean, *Nature*, *401*, 360–363.

Schickedanz, P. T., and E. G. Bowen (1977), The computation of climatological power spectrum, *J. Appl. Meteorol.*, *16*, 359–367.

Suzuki, R., S. K. Behera, S. Iizuka, and T. Yamagata (2004), Indian Ocean subtropical dipole simulated using a coupled general circulation model, *J. Geophys. Res.*, *109*, C09001, doi:10.1029/2003JC001974.

Thompson, D. W. J., and J. M. Wallace (2000), Annular modes in the extratropical circulation. Part I: Month-to-month variability, *J. Clim.*, *13*, 1000–1016.

Wallace, J. M., and D. S. Gutzler (1981), Teleconnections in the geopotential height field during the Northern Hemisphere winter, *Mon. Weather Rev.*, *109*, 784–812.

Wallace, J. M., C. Smith, and C. S. Bretherton (1992), Singular value decomposition of wintertime sea surface temperature and 500-mb height anomalies, *J. Clim.*, *5*, 561–576.

Wang, B., and Q. Zhang (2002), Pacific-East Asian teleconnection. Part II: How the Philippine Sea anomalous anticyclone is established during El Niño development?, *J. Clim.*, *15*, 3252–3265.

Wang, B., R. Wu, and X. Fu (2000), Pacific-East Asia teleconnection: How does ENSO affect East Asian climate?, *J. Clim.*, *13*, 1517–1536.

Wang, B., R. Wu, and T. Li (2003), Atmosphere-warm ocean interaction and its impacts on Asian-Australian monsoon variation, *J. Clim.*, *16*, 1195–1211.

Wang, H. (2005), The circum-Pacific teleconnection pattern in meridional wind in the high troposphere, *Adv. Atmos. Sci.*, *22*, 463–466.

Yang, S., K.-M. Lau, and K.-M. Kim (2002), Variations of the East Asian jet stream and Asian-Pacific-American winter climate anomalies, *J. Clim.*, *15*, 306–325.

Zhang, R., A. Sumi, and M. Kimoto (1996), Impact of El Niño on the East Asian monsoon: A diagnostic study of the 86/87 and 91/92 events, *J. Meteorol. Soc. Jpn.*, *74*, 49–62.

Q. Yang, Laboratory of Weather and Climate, Jiangsu Meteorological Institute, No. 2, Beijiguo, Nanjing 210008, China. (yqm0305@263.net)